Numerical Simulation and Modelling of the Forces Acting on Single and Multiple Non-Spherical Particles

Rafik Ouchene, Amine Chadil, Pascal Fede, Mohammed Khalij, Anne Tanière, Stéphane Vincent, Jean-Luc Estivalèzes, Boris Arcen

Proceedings of Proceedings of the ASME 2014 4th Joint US-European Fluids Engineering Division Summer Meeting and 11th International Conference on Nanochannels, Microchannels, and Minichannels
FEDSM2014
August 3-7, 2014, Chicago, Illinois, USA

FEDSM2014-22244

NUMERICAL SIMULATION AND MODELLING OF THE FORCES ACTING ON SINGLE AND MULTIPLE NON-SPHERICAL PARTICLES

Rafik Ouchene
Université de Lorraine
CNRS, LEMTA, UMR 7563
Vandoeuvre-lès-Nancy, FR-54500, France
Email: rafik.ouchene@univ-lorraine.fr

Amine Chadil
Université de Toulouse
INPT, UPS, CNRS UMR 5502
Toulouse, FR-31400, France
Email: amine.chadil@imft.fr

Pascal Fede*
Université de Toulouse
INPT, UPS, CNRS UMR 5502
Toulouse, FR-31400, France
Email: pascal.fede@imft.fr

Mohammed Khalij
Université de Lorraine
CNRS, LEMTA, UMR 7563
Vandoeuvre-lès-Nancy, FR-54500, France
Email: mohammed.khalij@univ-lorraine.fr

Anne Tanière
Université de Lorraine
CNRS, LEMTA, UMR 7563
Vandoeuvre-lès-Nancy, FR-54500, France
Email: anne.taniere@univ-lorraine.fr

Stéphane Vincent
Institut Polytechnique de Bordeaux
University of BORDEAUX 1
I2M Laboratory, UMR CNRS 5295
Pessac, FR-33607, France
Email: Stephane.Vincent@enscbp.fr

Jean-Luc Estivalezès
Université de Toulouse
INPT, UPS, CNRS UMR 5502
Toulouse, FR-31400, France
Email: jean-luc.estivalezes@imft.fr

Boris Arcen
Université de Lorraine
CNRS, LRGP, UMR 7563
Nancy, 54001, France
Email: boris.arcen@univ-lorraine.fr

ABSTRACT

The paper deals with gas-solid turbulent flows carrying non-spherical particles. The main objective of the present paper is to compute the hydrodynamics forces on non-spherical particles as a function of the particle orientation, for different particle shapes and a large range of particle Reynolds number. Two Direct Numerical Simulations at the scale of the particle are used, i.e. a body-fitted approach and a viscous penalty approach, in the case of a uniform flow with a single ellipsoidal particle. Results are compared with several correlations from the literature and a new proposal for the drag coefficient is given. The study is then extended to the case of a lattice of non-spherical particles to measure the pressure drop and to connect it with the drag coefficient.

INTRODUCTION

Gas-solid turbulent flows carrying non-spherical particles are found in many practical applications such as pneumatic conveying, paper manufacturers, or biomass combustion. The numerical simulations of such applications are usually performed using an Euler-Euler approach requiring constitutive relationships for the particle-fluid momentum transfer. An Eulerian-Lagrangian formulation can also be used where the carrier phase flow is obtained from the Navier-Stokes equations while the mo-

tion of each particle is modelled from the particle equation motion. Whatever the modeling point of view, the knowledge of the forces acting on particles is necessary to model the momentum transfer at the solid/fluid interface in Eulerian approach and for having a correct description of particle trajectories in the Lagrangian approach. Many studies were devoted to the modelling of these forces when the particles are spherical and then an open issue is the forces acting on non-spherical particles.

Since 1920, many theoretical and experimental work on the hydrodynamic forces on non-spherical particles in the literature have been published. For instance, Jeffery (1922) [1] and Brenner (1963) [2] theoretically derived the forces acting on particles of different shapes in Stokes regime and for different flow conditions. Their results are often used to model the motion of non-spherical particles. Unfortunately, these studies have to be restricted to the Stokes regime [3]. The use of these low-Reynolds number models for the forces acting on non-spherical particles is almost unavoidable since there are few available proposals which predict all the coefficients (drag, lift, and torque coefficients) as a function of the particle orientation, for different particle shapes and a large range of particle Reynolds number. In addition, Chhabra et al. (1999) [4] showed that some discrepancies exist between the correlations found in the literature. They were the first to compile and classify the most used correlations before 1999. Recently, a comparison of two recent correlations with data given by a body-fitted computation was conducted by Ouchène et al.(2013) [5]. These correlations were developed by Hölzer and Sommerfeld (2008) [6] and Zastawny et al. (2011) [7] from DNS data (obtained using an immersed boundary method). Ouchène et al.(2013) [5] showed that the correlations do not predict accurately the drag coefficient for the considered range of aspect ratio and particle Reynolds number.

In order to examine more thoroughly the accuracy of these correlations, Direct Numerical Simulations of the flow around non-spherical particles were conducted using two different numerical methods (body-fitted and fictitious domain). Firstly, the two numerical techniques are validated by comparison of the DNS results with the theoretical results given by Brenner (1963) [2]. The DNS results, obtained from body-fitted simulations, are then compared with the correlations from the literature ([6], [7]). The effect of the aspect ratio, the attack angle, and the particle Reynolds number on the hydrodynamics coefficients will be examined. In a second part, the interaction of a uniform flow with a lattice of non-spherical particles (with different solid volume fractions) is studied.

The present paper is organized as follow. The first section is devoted to the description of the numerical methods. Sections two and three present the flow around a single particle and through multiple particles, respectively.

NUMERICAL METHODS

The Direct Numerical Simulation (DNS) of a particulate flow transported by turbulent flows is challenging because of the motion of the particles. The most direct approach is the implementation of an unstructured body-fitted grid to simulate the fluid in the two-phase particle flow [8, 9]. Building such a three-dimensional mesh is not easy and requires automatic mesh generators as the solid particles move according to time and space. The remeshing process at each calculation step can be very difficult to manage automatically when global shape of the fluid-solid interface is complex. The second solution consists in the use of the fictitious domain approach where the mesh is not adapted to the fluid-solid interfaces. There are several methods based on this approach: the Mirroring Immersed Boundary Method [7, 10], the Lattice Boltzmann Method [6] and Viscous Penalty Method [11, 12] which is used in this study, to name a few. The difficulty lies in taking the presence of particles in the fluid into account whose interfaces are not explicitly tracked by the non conforming mesh. In the present work, two approaches are used for the numerical simulation of a single particle and of multiple particles. The choice of the development of the fictitious domain approach is that the next step of the project will be to perform DNS of particle-laden flows.

Body-fitted approach

In the present study, it is assumed that the flow is isothermal, incompressible, and the fluid is Newtonian. This flow is thus governed by the continuity and Navier-Stokes equations:

$$\nabla \cdot \mathbf{u} = 0, \tag{1}$$

$$\frac{\partial \mathbf{u}}{\partial t} + (\mathbf{u} \cdot \nabla)\mathbf{u} = -\frac{1}{\rho_f}\nabla p + \nu \Delta \mathbf{u}, \tag{2}$$

where $\mathbf{u}(\mathbf{x},t)$ represents the fluid velocity, p is the pressure, ρ_f is the fluid density, ν the kinematic viscosity. As mentioned before, for the range of particle Reynolds numbers studied, the flow remains in steady-state, therefore, the unsteady term in the Navier-Stokes equations is neglected. The steady-state simulations are performed using the CFD code Ansys Fluent. Centered scheme are used for discretizing all the numerical fluxes in the Navier-Stokes equations. The problem of the coupling between velocity and pressure is tackled with a Semi-Implicit Method for Pressure-Linked Equations (SIMPLE) [13]. In the body-fitted approach, the fluid volume is discretized into unstructured tetrahedral control volumes while a triangular surface mesh is used for the surface of the particle immersed in the fluid. The mesh surface of the particle is sufficiently fine to give an accurate integration of the forces acting on the particle surface. An example of the volume and surface meshes is presented in Fig. 1.

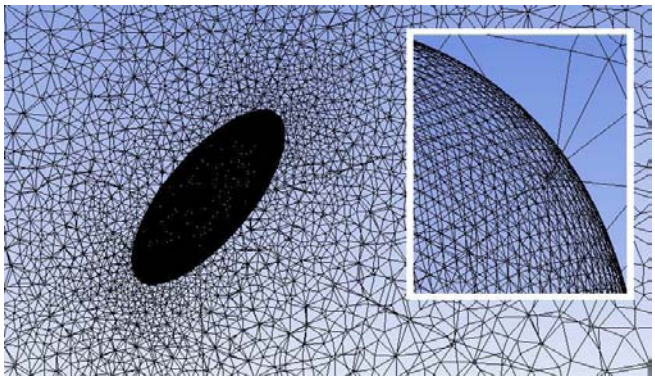

FIGURE 1. COMPUTATIONAL MESH FOR FLOW PAST AN ELLIPSOIDAL PARTICLE

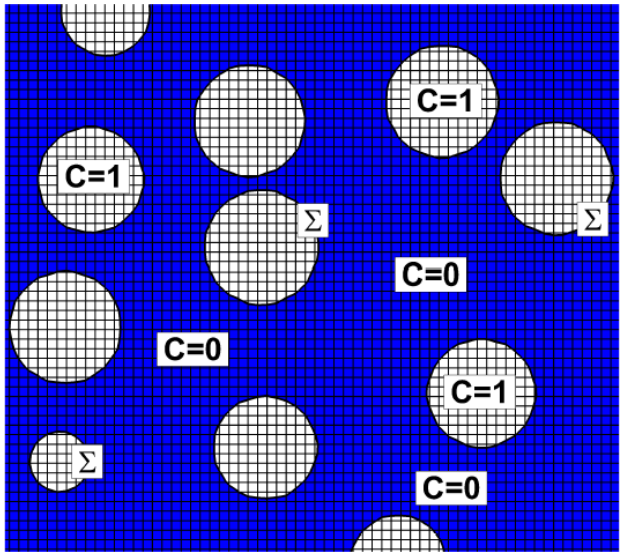

FIGURE 2. FICTITIOUS DOMAIN

Viscous penalty method

The fictitious domain method consists in introducing a phase function C to locate each medium and to formulate a global model valid in the fluid and in the solid parts of the flow. According to the local value of C, the physical characteristics and the conservation equations are adapted to fulfill the correct physical behaviour. By definition, $C = 1$ in the solid, $C = 0$ in the fluid and the interface Σ between the fluid and solid phases is associated to $C = 0.5$ (see Fig. 2). The Viscous Penalty Method consists in penalizing the viscosity in the meshes contained in the solid to have the rigid behaviour. Incompressible two-phase flows is modelled by solving the incompressible Navier-Stokes equations with a phase function C describing the particle phase shape evolutions through an advection equation on the corresponding phase function. As explained by Kataoka [14], the resulting set of equations takes implicitly into account the jump relations at the interface and the fluid-solid interface modulations are taken into account in an Eulerian manner by the advection equation on C. Finally, the set of equations writes

$$\nabla \cdot \mathbf{u} = 0 \tag{3}$$

$$\rho \left[\frac{\partial \mathbf{u}}{\partial t} + (\mathbf{u} \cdot \nabla)\mathbf{u} \right] = -\nabla p + \rho \mathbf{g} + \nabla \cdot \left[\mu \left(\nabla \mathbf{u} + \nabla^T \mathbf{u} \right) \right] + \mathbf{F}_{si} \tag{4}$$

$$\frac{\partial C}{\partial t} + \mathbf{u} \cdot \nabla C = 0 \tag{5}$$

where $\mathbf{u}$ is the velocity, p the pressure, t the time, $\mathbf{g}$ the gravity vector, ρ and μ respectively the density and the viscosity of the equivalent fluid. The two-way coupling between particle and fluid is ensured in the momentum equations by using a decomposition of the viscous stress tensor and by playing on the order of magnitude of the viscosity in the solid phase. Typically, the viscosity coefficients are 2 to 3 orders of magnitude larger in the solid than in the surrounding fluid. The interaction force $\mathbf{F}_{si}$ is a four-way coupling term that accounts for particle-particle interactions (collision, lubrication). It is discarded here as the particles are static. The incompressibility condition is ensured by a augmented Lagrangian method. For more details on this technique please refer to [11, 12].

Computation of the forces acting on the particles

Basically, the forces acting on the particle are evaluated with

$$\mathbf{F} = -\int_S p\mathbf{n}\, dS + \int_S \tau \cdot \mathbf{n}\, dS \tag{6}$$

where τ is the viscous stress tensor. Assuming that the main flow is directed along the $\mathbf{x}$-axis, the drag force is then given by $F_D = \mathbf{F} \cdot \mathbf{x}$ and the lift force by $F_L = \mathbf{F} \cdot \mathbf{y}$. These two forces have two contributions: first a component due to the effect of the pressure and second due to the friction of the gas on the particle surface.

As in body-fitted approach the fluid-particle interface is explicitly defined, it is possible to compute the fluid stress tensor at the particle surface. In contrast, when using immersed boundary approach the properties of the fluid are not defined at the surface of the particle. A straightforward manner to compute forces in fictitious domain approach consists in associating a triangular surface grid to the barycenter and orientation of the particle and extrapolating the fluid variables (pressure, viscous stress tensor) from the neighboring cells to the surface elements describing the particle surface. This particle grid is also used to define the eulerian Navier-Stokes cells belonging to the particle (solid phase) of to the fluid phase. This surface particle mesh is superimposed

to the mass and momentum structured solving mesh. It allows to define C accurately according to ray casting procedures [11]. It is also used to integrate the interaction forces between the fluid and the particles.

The drag and lift forces are expressed in terms of drag and lift coefficients, C_D and C_L respectively. Using such coefficients, the forces write $F_D = 1/2\rho_f U_\infty^2 S_p C_D$ and $F_L = 1/2\rho_f U_\infty^2 S_p C_L$ where S_p is the surface of the particle facing the flow. In case of spheres such a surface is well-defined as $S_p = \pi d_p^2/4$. However, when non-spherical particles are considered the uniqueness of such a surface is no longer valid and the choice of the surface is still an open issue. Here, the surface is defined as in previous studies [6,7], it is based on the surface of spherical particle facing the flow but having a diameter, d_{eq} defined such as the equivalent spherical particle has the same volume than the non-spherical particle. Then the drag and lift forces write:

$$F_D = \frac{1}{2}\rho_f U_\infty^2 \left(\frac{\pi d_{eq}^2}{4}\right) C_D \tag{7}$$

$$F_L = \frac{1}{2}\rho_f U_\infty^2 \left(\frac{\pi d_{eq}^2}{4}\right) C_L\,. \tag{8}$$

As only ellipsoidal particles are investigated the connexion of d_{eq} with the two axis the ellipsoid is $d_{eq} = 2\sqrt[3]{ab^2}$ (see Fig. 3). In DNS the drag and lift forces are both computed accordingly to the numerical approach (body-fitted or fictitious domain) and the drag and lift coefficients are calculated with Eqn. 7 & Eqn. 8.

FLOW ARROUND A SINGLE PARTICLE

Geometry and boundary conditions

The particle shapes are given by Fig. 3. Several aspect ratios ($w = \frac{a}{b}$) are investigated in this study. This is the typical range encountered in many practical processes such as coal combustion.

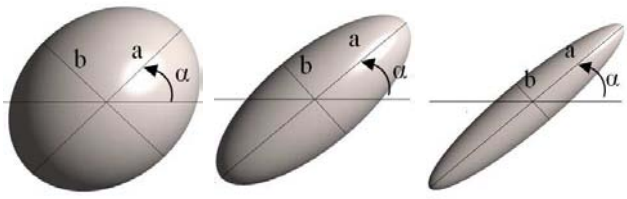

FIGURE 3. PARTICLE SHAPES. ELLIPSOIDS WITH DIFFERENT ASPECT RATIOS, RESPECTIVELY FROM LEFT TO RIGHT w= 1.25, 2.5 AND 5.

Besides, even if the flow remains in steady-state, the wake

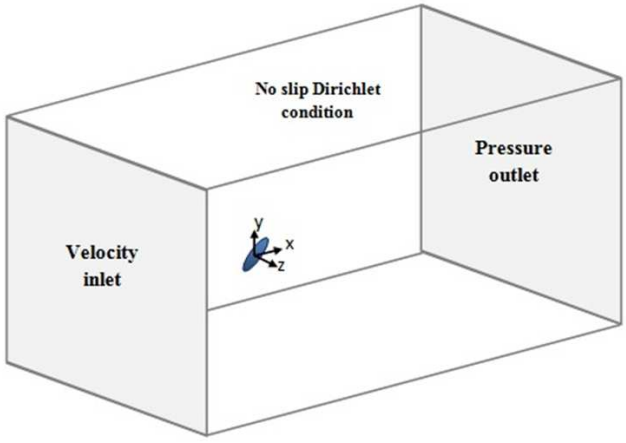

FIGURE 4. GEOMETRICAL CONFIGURATION AND BOUNDARY CONDITIONS.

starts to become asymmetric at $Re_p \approx 200$ [6, 7, 15]). Hence, for a better estimation of the hydrodynamic forces, it was required to consider simulation in a complete 3D configuration. Thus, in the considered simulations the particle is supposed fixed and immersed in a tridimensional uniform flow. The geometrical configuration (Fig. 4) is a parallelepiped box. The size of the box has been determined to prevent any disturbance of the flow due to boundary conditions, especially in the boundary layer. From a practical point of view, these dimensions were imposed by the case Re_p = 0.1 resulting in a greater boundary layer where the particle is located transversely to the flow. In addition, the length of the computational box was set to leave an adequate distance for the development of the wake. The boundary conditions are presented in Fig. 4. A constant velocity inflow condition is imposed at the inlet boundary whereas homogeneous Neumann conditions are chosen at the outlet. On lateral boundaries, no-slip Dirichlet conditions are specified. Three different volume meshes (500 000, 1 million, 2 millions) were tested, in the body-fitted approach, in order to ensure that the results are mesh independent for Re_p= 290. Similar results of drag, lift and torque coefficients are obtained whatever the mesh used. Thus, the number of cells chosen for all the simulation is about 500 000. It has to be noted that the boundary layer is always represented by at least 20 nodes.

In case of spherical particles, the fictitious domain approach requires up to 12 cells in a particle diameter for predicting accurately the flow at low Reynolds number. Up to now the sensitivity of the method with respect to the mesh has not been established for non-spherical particle. Then the mesh is based on the criteria defined for spherical particle. This restriction on the mesh size leads to use a small domain for performing the numerical simulation with fictitious approach. The Table 1 gives the size of the domain used for both the body-fitted and the fictitious domain

approaches.

TABLE 1. SIZE OF THE DOMAIN USED IN DNS FOR $w = 2.5$ AND $Re_p = 0.1$

	Body-fitted	Fictitious domain
L_x/d_{eq}	75.6	20
L_y/d_{eq}	50.4	20
L_z/d_{eq}	50.4	20
$L_x/2b$	205.2	20
$L_y/2b$	136.8	20
$L_z/2b$	136.8	20

Validation for $Re_p \to 0$

Figure 5 shows the drag and lift coefficients extracted from the present DNS computations (body-fitted and fictitious domain approaches) as well as the DNS results obtained by Zastawny et al. [7] using an Immersed Boundary approach. As the Reynolds number is quite low (approximately 0.1 in all numerical simulations), the analytical solution proposed by Brenner [2] is valid. Indeed, for $Re_p \to 0$ Brenner [2] proposed expressions for the drag and lift coefficients for any angle of attack. These coefficients are written in terms of the values for $\alpha = 0°$ and $\alpha = 90°$ as

$$C_D = C_{D,\alpha=0°} + (C_{D,\alpha=90°} - C_{D,\alpha=0°})\ \sin(\alpha)^2\,, \tag{9}$$

$$C_L = (C_{D,\alpha=90°} - C_{D,\alpha=0°})\ \sin(\alpha)\ \cos(\alpha)\,. \tag{10}$$

The asymptotic values for $\alpha = 0°$ and $\alpha = 90°$ are written as a deviation from the coefficient of a sphere:

$$C_{D,\alpha=0°} = C_{D,sphere} K_{\alpha=0°}\,, \tag{11}$$

$$C_{D,\alpha=90°} = C_{D,sphere} K_{\alpha=90°}\,. \tag{12}$$

The drag coefficient for a sphere at low Reynolds number is $C_{D,sphere} = 24/Re_p$ and the coefficients $K_{\alpha=0}$ and $K_{\alpha=90}$ was analytical computed by Brenner [2], it takes the following form:

$$K_{\alpha=0°} = \frac{8}{3} w^{-1/3} \times \left[-\frac{2w}{w^2-1} + \frac{2w^2-1}{(w^2-1)^{3/2}} \ln\left(\frac{w+\sqrt{w^2-1}}{w-\sqrt{w^2-1}} \right) \right]^{-1} \tag{13}$$

$$K_{\alpha=90°} = \frac{8}{3} w^{-1/3} \times \left[\frac{w}{w^2-1} + \frac{2w^2-3}{(w^2-1)^{3/2}} \ln\left(w+\sqrt{w^2-1} \right) \right]^{-1} \tag{14}$$

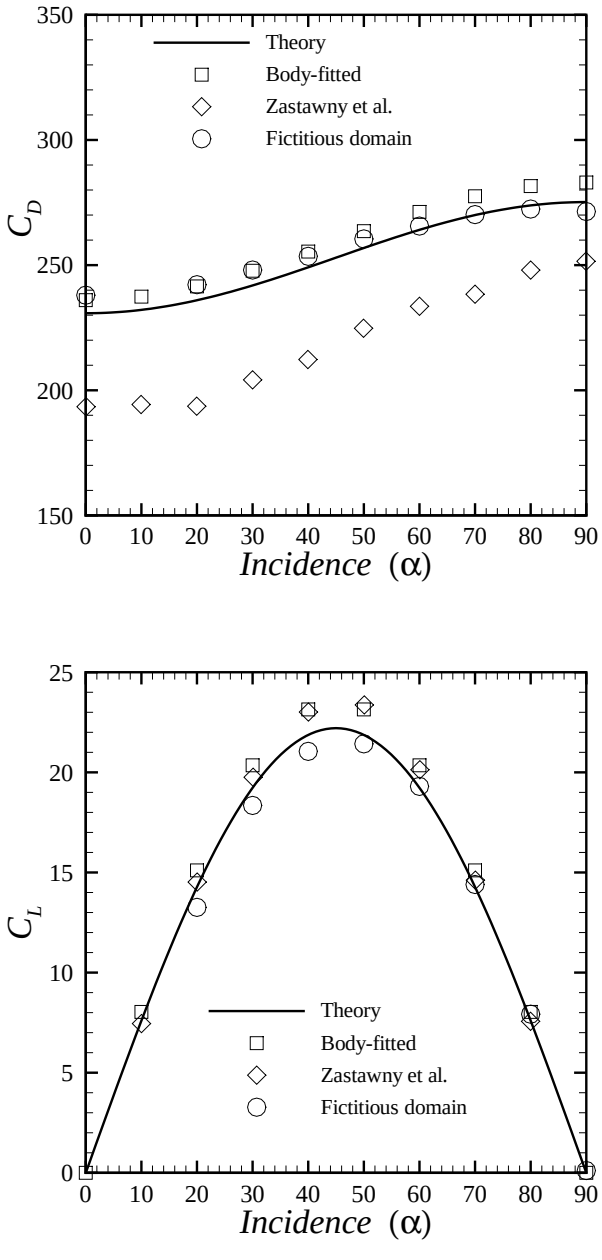

FIGURE 5. DRAG AND LIFT COEFFICIENTS MEASURED FOR AN ELLIPSOID WITH AN ASPECT RATIO w=2.5 AND FOR A LOW REYNOLDS NUMBER Re_p = 0.1

Figure 5 shows that the drag and lift coefficients obtained from the present DNS (body-fitted and fictitious domain approaches) are in good accordance with the theoretical expression whatever the incidence angle. The body-fitted approach slightly overestimates the drag coefficient over the incidence angle range while the fictitious domain approach overestimates this coefficient for low incidence angle and then gives results almost identical to the theory. Concerning the lift coefficient, the body-fitted approach also slightly overestimates the theoretical results. The fictitious domain approach generally underestimates slightly the lift coefficient. The drag and lift coefficients provided by Zastawny et al. [7] are also plotted on this figure. It can be observed that their DNS results for the drag coefficient are far from the theory while the evolution of the lift coefficient as a function of the incidence angle is almost identical to the one given by the body-fitted approach. The deviations from the computational results and theory are shown in Tab. 2. As previously observed, the mean deviation from theory is of the order of 2% for the present body-fitted and fictitious domain approaches. This deviation is 7 times higher for the results provided by Zastawny et al. (2012). The maximum deviations for the three computations are close to the mean deviations. The present computations being validated against Brenner's theoretical results, we present in the next section the drag coefficient at higher Reynolds number. These results were obtained using the body-fitted approach.

TABLE 2. DEVIATIONS FROM THE THEORICAL RESULTS OF BRENNER FOR AN ELLIPSOID WITH AN ASPECT RATIO w=2.5 AT Re_p=0.1

	Mean relative deviation (%)	Maximum relative deviation (%)
Fictitious method	1.53	3.02
Body-fitted	2.62	2.85
Zastawny et al. (2012)	14.0	19.5

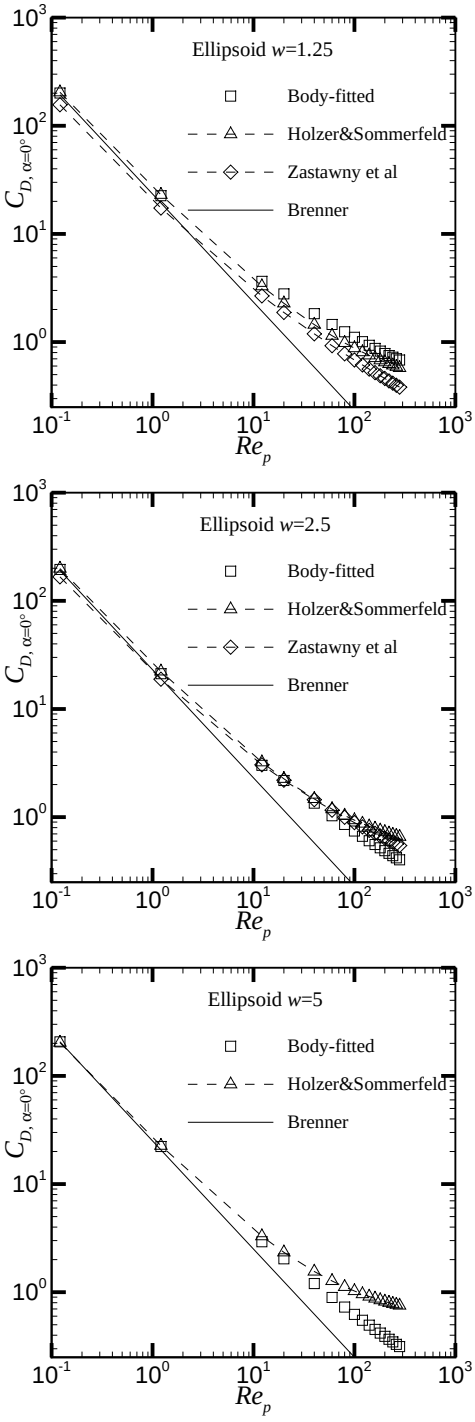

FIGURE 6. DRAG COEFFICIENT WITH RESPECT TO THE REYNOLDS NUMBER FOR $\alpha = 0°$. COMPARISON WITH EXISTING CORRELATIONS.

Effect of the particle Reynolds number

Figures 6 & 7 show the effect of the particle Reynolds number on the drag coefficient for $\alpha = 0°$ and $\alpha = 90°$. Two correlations are reported. First, Hölzer & Sommerfeld [6] proposed the

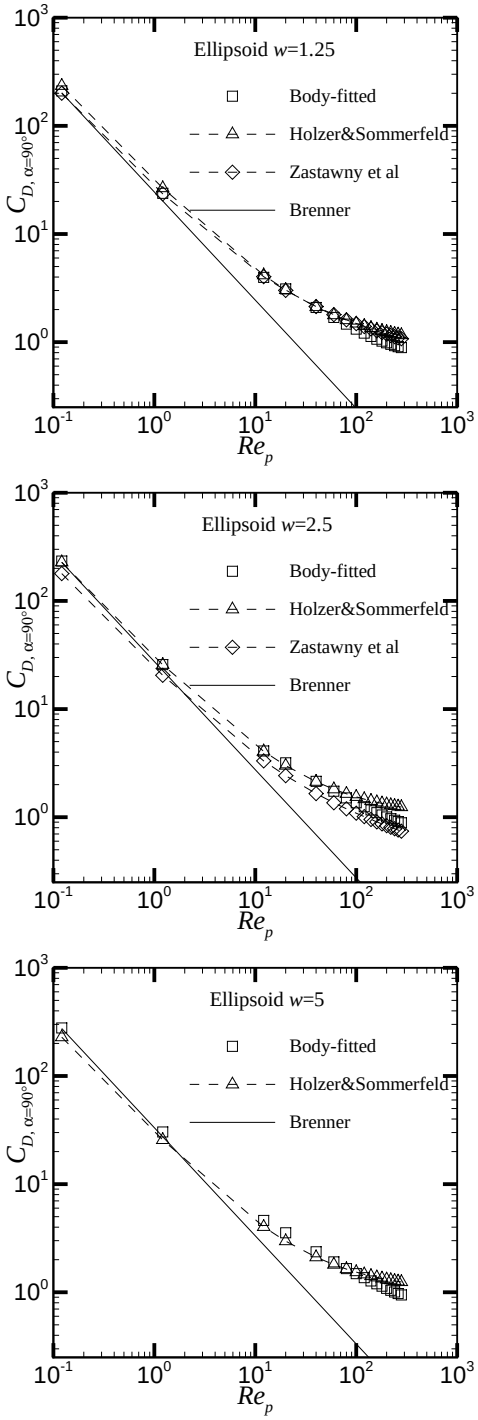

FIGURE 7. DRAG COEFFICIENT WITH RESPECT TO THE REYNOLDS NUMBER FOR $\alpha = 90°$. COMPARISON WITH EXISTING CORRELATIONS.

following correlation

$$C_D = \frac{8}{Re_p}\frac{1}{\sqrt{\phi_\perp}} + \frac{16}{Re_p}\frac{1}{\sqrt{\phi}} + \frac{3}{\sqrt{Re_p}}\frac{1}{\phi^{0.75}} + 0.42\ 10^{0.4(-\log\phi)^{0.2}}\frac{1}{\phi_\perp}\ , \tag{15}$$

where ϕ is the lengthwise sphericity and $\phi_\perp$ crosswise sphericity. This correlation has been established from the analysis of many experiments. The second correlation has been proposed by Zastawny et al. [7] from the analysis of their results with Immersed Boundary method. They proposed

$$C_{D,\alpha=0°} = \frac{a_1}{{Re_p}^{a_2}} + \frac{a_3}{{Re_p}^{a_4}}\ , \tag{16}$$

$$C_{D,\alpha=90°} = \frac{a_5}{{Re_p}^{a_6}} + \frac{a_7}{{Re_p}^{a_8}}\ . \tag{17}$$

$$\tag{18}$$

For the intermediate value of the drag coefficient they write:

$$C_D = C_{D,\alpha=0°} + (C_{D,\alpha=90°} - C_{D,\alpha=0°})\ \sin(\alpha)^{a_0}\ . \tag{19}$$

where a_0, a_1, a_2, a_3, a_4, a_5, a_6, a_7, and a_8 are coefficients fitted from the DNS performed with Immersed Boundary method. Zastawny et al. [7] proposed also the following correlation for the lift force

$$C_L = \frac{b_1}{{Re_p}^{b_2}}\frac{b_3}{{Re_p}^{b_4}}\ \sin(\alpha)^{b_5+b_6{Re_p}^{b_7}}\ \cos(\alpha)^{b_8+b_9{Re_p}^{b_{10}}} \tag{20}$$

where b_0 to b_{10} are model coefficients.

As expected, Figs. 6 & 7 show that the drag coefficient is decreasing for increasing Reynolds particle number. For small particle Reynolds number, the body-fitted DNS and the correlations tend towards the solution proposed by Brenner [2]. For $w = 1.25$, the correlation proposed by Hölzer & Sommerfeld [6] is in accordance with the body-fitted DNS even for large particle Reynolds number. In contrast, for larger aspect ratio, the correlation overestimates the drag coefficient for $\alpha = 0°$. For $\alpha = 90°$, the two correlations are in accordance with the body-fitted results. Mean and maximum relative deviations $err = [|C_D(simulation) - C_D(correlation)|/C_D(simulation)] \times 100$ are gathered in Tab. 3. A significant deviation from the present numerical results is noted, especially for elongated particles (high aspect ratio). The mean relative deviation is generally over 10% while the maximum relative deviation is over 20% in most cases. Based on these results, we decided to propose a new correlation in order to more accurately predict the drag coefficient of ellipsoidal particles. The new correlation is presented in the next section.

TABLE 3. DEVIATIONS OF THE LITERATURE CORRELATION FROM THE RESULTS OF THE PRESENT SIMULATIONS

Deviations & Aspect ratios		Hölzer & S		Zastawny	
Deviations	w	α=0°	α=90°	α=0°	α=90°
Mean relative deviation (%)	w=1.25	7.5	21.3	8.6	16.9
	w=2.5	32.5	19.0	18.2	11.9
	w=5	46.7	11.4	-	-
Maximum relative deviation (%)	w=1.25	16.1	39.8	20.8	21.2
	w=2.5	63.5	39.9	19.2	22.0
	w=5	83.5	22.9	-	-

New correlation

The approach used to determine the new correlation of the drag coefficient is based on the four following points:

1. Whatever the particle Reynolds number, the drag coefficient evolves between $\alpha = 0°$ and $\alpha = 90°$ as a sine function [2].

2. The drag coefficients $\alpha = 0°$ and $\alpha = 90°$ evolve as a function of the particle Reynolds number.

3. As Loth (2008) [16], the aspect ratio w is taken to be the main shape parameter of the ellipsoids.

4. The correlation has to degenerate to the Schiller & Naumann [17] correlation for $w = 1$ (sphere).

From these considerations, the proposed correlation for the drag coefficient has the following form:

$$C_{D,\alpha=0°} = \frac{24}{Re_p}[F_{\alpha=0°}(w) + 0.15 G_{\alpha=0°}(w) Re_p^{0.687}], \quad (21)$$

$$C_{D,\alpha=90°} = \frac{24}{Re_p}[F_{\alpha=90°}(w) + 0.15 G_{\alpha=90°}(w) Re_p^{0.687}], \quad (22)$$

where $F_{\alpha=0°}(w)$, $G_{\alpha=0°}(w)$, $F_{\alpha=90°}(w)$, $G_{\alpha=90°}(w)$ are correction factors. For spherical particles, there is no dependence on the orientation, then $F = G = 1$ in order to recover the Schiller & Naumann correlation. For non-spherical particles, the correction factors, $F_{\alpha=0°}(w)$ and $F_{\alpha=90°}(w)$, are taken from Brenner [2] so that $F_{\alpha=0°}(w) = K_{\alpha=0°}$ and $F_{\alpha=90°}(w) = K_{\alpha=90°}$ both given by Eqn. 13 & Eqn. 14. The two functions $G_{\alpha=0°}(w)$, $G_{\alpha=90°}(w)$ are approximated from the present body-fitted DNS. The fitting procedure leads to the following functions:

$$G_{\alpha=0°}(w) = w^{-0.57}, \quad (23)$$

$$G_{\alpha=90°}(w) = w^{0.2}. \quad (24)$$

The new correlations of the drag coefficient at the both incidence angles $\alpha = 0°$ and $\alpha = 90°$ are:

$$C_{D,\alpha=0°} = \frac{24}{Re_p}[K_{\alpha=0°} + 0.15 w^{-0.57} {Re_p}^{0.687}], \quad (25)$$

$$C_{D,\alpha=90°} = \frac{24}{Re_p}[K_{\alpha=90°} + 0.15 w^{0.2} {Re_p}^{0.687}]. \quad (26)$$

Figures 8 & 9 compare the proposed correlation with the body-fitted DNS results for the three aspect ratios. A good accordance is noted. In order to examine the accuracy of the proposed correlation, the mean and maximum deviations of this formula from the body-fitted DNS results are given in Tab. 4.

TABLE 4. DEVIATIONS OF THE PRESENT CORRELATION FROM THE RESULTS OF SIMULATIONS

Deviations & Aspect ratios		Present correlation Eqn. 25	
Deviations	w	α=0°	α=90°
Mean relative deviation (%)	w=1.25	9.3	10.8
	w=2.5	4.4	5.4
	w=5	2.6	8.8
Maximum relative deviation (%)	w=1.25	13.2	17.7
	w=2.5	5.5	11.3
	w=5	5.0	13.51

For a better representation of the effect of the orientation for different particle Reynolds numbers, the computed drag coefficient is normalized by the drag coefficient obtained at the incidence angle $\alpha = 90°$. The results are presented in Fig. 10 where the ratio $\frac{C_{D,simulation}}{C_{D,\alpha=90°}}$ is plotted as a function of α for different aspect ratio, respectively. For each aspect ratio, we propose to test the extension of Brenner's formula at higher Reynolds number. Based on Brenner's methodology, it yields (Eqn. 27):

$$\frac{C_{D,simulation}}{C_{D,\alpha=90°,simulation}} = \frac{C_{D,simulation}}{C_{D,\alpha=90°,simulation}} + (1 - \frac{C_{D,simulation}}{C_{D,\alpha=90°,simulation}}) \sin(\alpha)^2. \quad (27)$$

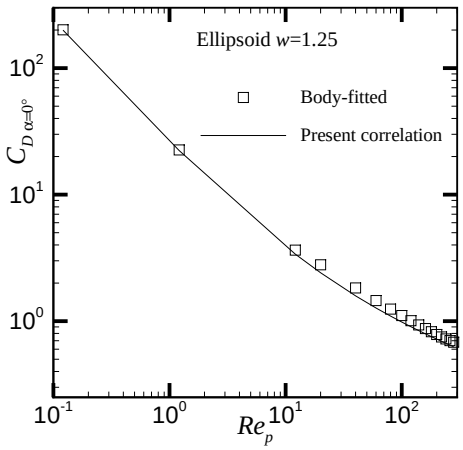

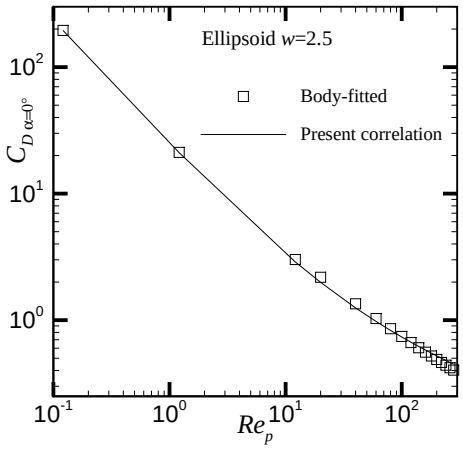

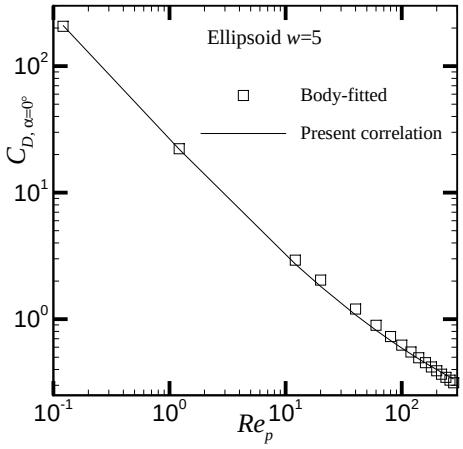

FIGURE 8. COMPARISON BETWEEN COMPUTATIONAL DRAG COEFFICIENT WITH THE PRESENT CORRELATION AT $\alpha = 0°$.

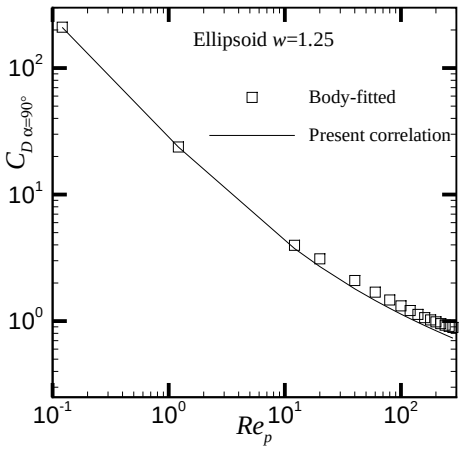

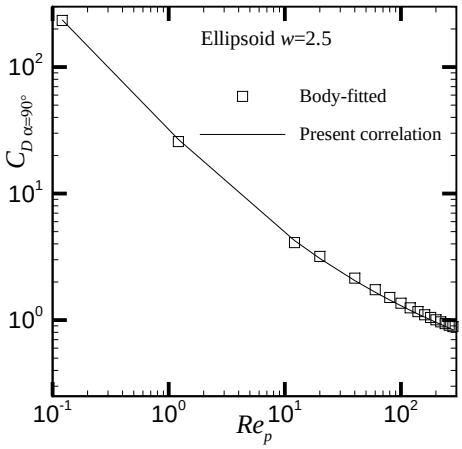

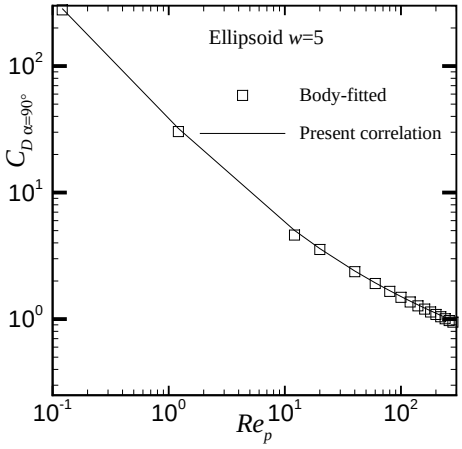

FIGURE 9. COMPARISON BETWEEN COMPUTATIONAL DRAG COEFFICIENT WITH THE PRESENT CORRELATION AT $\alpha = 90°$.

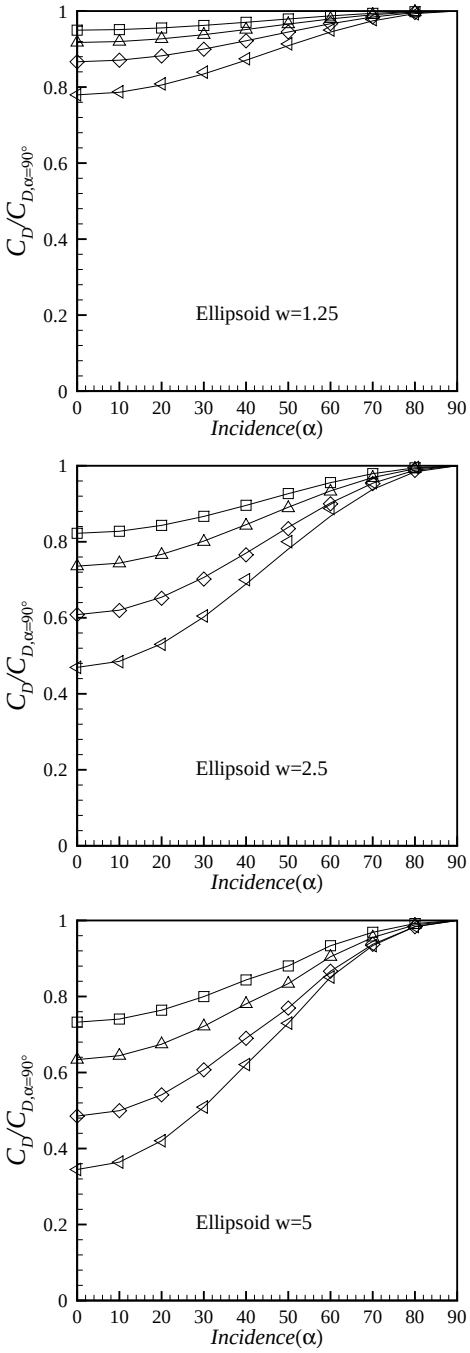

FIGURE 10. COMPARISON BETWEEN THE NORMALIZED DRAG COEFFICIENT AND THE NORMALIZED BRENNER'S FORMULA. □: Re_p=1.21; △: Re_p=10; ◇: Re_p=60; ◁: Re_p=240. CONTINOUS LINES: Eqn. 27.

Figure 10 shows the predictions of the correlation normalized by DNS measurements as defined by Eqn. 27 for several values of Reynolds number and for the three aspect ratios. Figure 10 shows that whatever the value of the particle Reynolds number, a similar trend with normalized Brenner's formula is retrieved, *i.e.* a monotonic increase as incidence angle increases. However, the influence of the incidence angle is seen to be less important when the particle Reynolds number decreases. The dependence to the aspect ratio is also observed. As the aspect ratio increases, the normalized drag coefficient decreases. The incidence angle has less influence on the normalized drag coefficient for the lowest aspect ratio (w=1.25) in comparison with the other ones. Quantitatively, the mean relative deviation is less than 1% for most cases. Hence, we confirm that Brenner's formula are still valid over the Stokes regime flow.

FLOW THROUGH MULTIPLE PARTICLES

Configuration overview

The domain is a box of length $40d_{eq} \times 5d_{eq} \times 5d_{eq}$ and the flow is directed to the axis **x**. The particles are located at the centre of the domain as shown in Fig. 11.

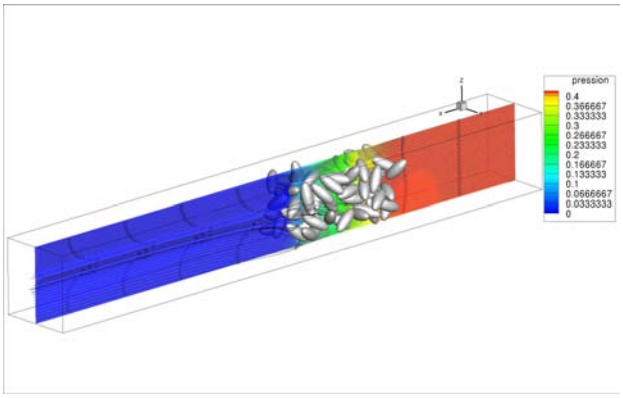

FIGURE 11. CONFIGURATION FOR MULTIPLE PARTICLES.

A uniform flow is imposed at the inlet located at $x = 0$ and a free outlet condition is considered at $x = 2L_x$. In $y-$ and $z-$ direction symmetry conditions are assumed at the boundaries. The gas is air under standard thermodynamic conditions so that the density is $\rho = 1.2kg/m^3$ and the dynamic viscosity $\mu = 1.8 \times 10^{-5} Pa.s$. The fictitious domain DNS has been performed for two different aspect ratios (w =1.25 and 2.50), three different solid volume fractions (α_p=5%, 10% and 15%) and three Reynolds number (Re_p=1.0, 10.0 and 100.0). The centre of mass and the orientation of the particles are both randomly defined in order to prevent particle overlapping.

Topology of the flow

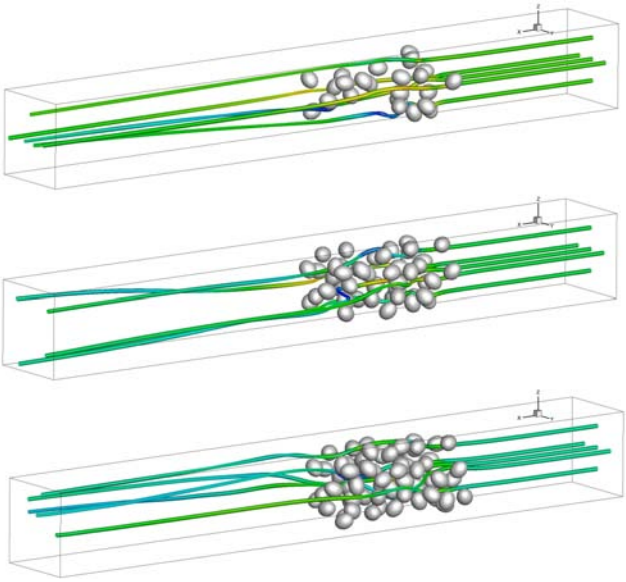

FIGURE 12. STREAMTRACE OF FLUID VELOCITY THROUGH A NON-SPHERICAL PARTICLE FOR $w = 1.25$ AND $Re_p = 100.0$. FROM TOP TO BOTTOM: α_p=5%, 10% AND 15%.

The structure of the flow is shown in Figs. 12, 13 & 14. As expected when increasing the solid volume fraction the distortion of the streamtrace is increasing. The contour of the velocity magnitude normalized by the inlet velocity is shown in Fig. 13. As also expected low-velocity regions are observed behind the particles as interaction between the particles.

The normalized vorticity magnitude shown in Fig. 14 exhibits the formation of wakes. The formation of wakes is related to the particle Reynolds number. The effect of Re_p on the case where the solid volume fraction is α_p =15% and for the aspect ratio $w = 1.25$ is shown by Fig. 15. Obviously, for small Reynolds number the vorticity is very small and located very close to the particle. In contrast for a Reynolds number of 100 long-range wakes appears and the Fig. 14 clearly shows the interaction of the particles with the wake due to the presence of neighbouring particles. The effect of the aspect ratio on the formation of vorticity is presented in Fig. 16 for $Re_p = 100$ and α_p =5%. Even if the maximum of vorticity is found for the largest aspect ratio, the role of the aspect ratio is not clear on the mechanism of production of wake. More investigations are required.

Pressure drop

In this section the pressure drop measured in fictitious domain DNS are shown. The aim is to do the same procedure than

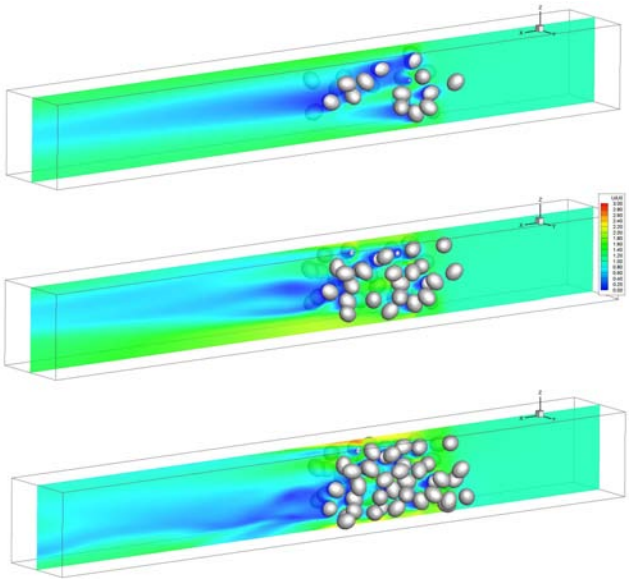

FIGURE 13. EFFECT OF THE SOLID VOLUME FRACTION ON THE NORMALIZED (BY INLET VELOCITY) VELOCITY MAGNITUDE. NON-SPHERICAL PARTICLE ARRAY FOR $w = 1.25$ AND $Re_p = 100.0$. FROM TOP TO BOTTOM: α_p=5%, 10% AND 15%.

Ergun [18] who extracted the pressure drop from experiments and did the connection between the pressure drop and the drag coefficient. Such a methodology allows an indirect computation of the drag coefficient.

As expected the pressure drop increases for increasing solid volume fraction. The two low aspect ratios ($w = 1$ and $w = 1.25$) give nearly the same pressure drop for all investigated particle Reynolds number. In contrast, for $w = 2.5$ the pressure drop is found lower than the case of spheres or with a small aspect ratio. This trend comes probably from the orientation of the ellipsoidal particles that could be not strictly uniform.

CONCLUSIONS

The main aim of this study has been to assess the reliability of different numerical methods to compute the hydrodynamic coefficients linked to non-spherical particles as ellipsoids. The effect of the aspect ratio, the attack angle, and the particle Reynolds number on such hydrodynamic coefficients have been examined. Both methods have been compared in the Stokes regime for which a theoretical solution exists ([2]). Drag and lift coefficients have been compared to theoretical results but also compared to recent DNS computations [7]. Results show a very good accordance between Brenner's results and those issued from the body-fitted and fictitious domain approaches.
For higher Reynolds number, the results extracted from the body-fitted approach for a single particle have been used to propose

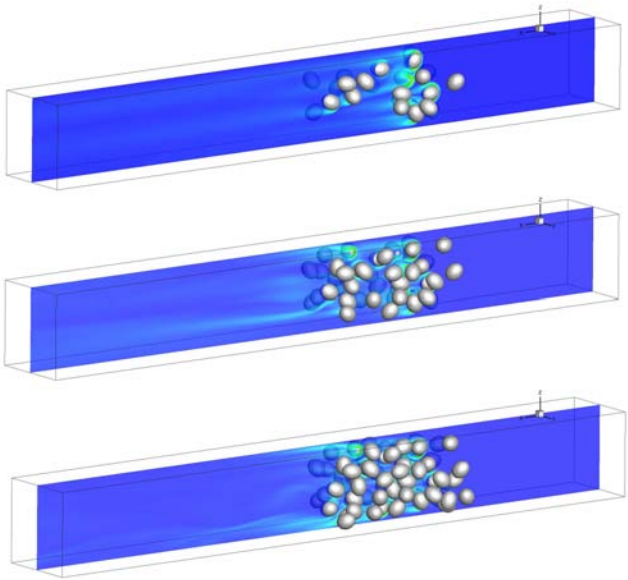

FIGURE 14. EFFECT OF THE SOLID VOLUME FRACTION ON THE NORMALIZED VORTICITY MAGNITUDE. NON-SPHERICAL PARTICLES ARRAY FOR $w = 1.25$ AND $Re_p = 100.0$. FROM TOP TO BOTTOM: α_p=5%, 10% AND 15%.

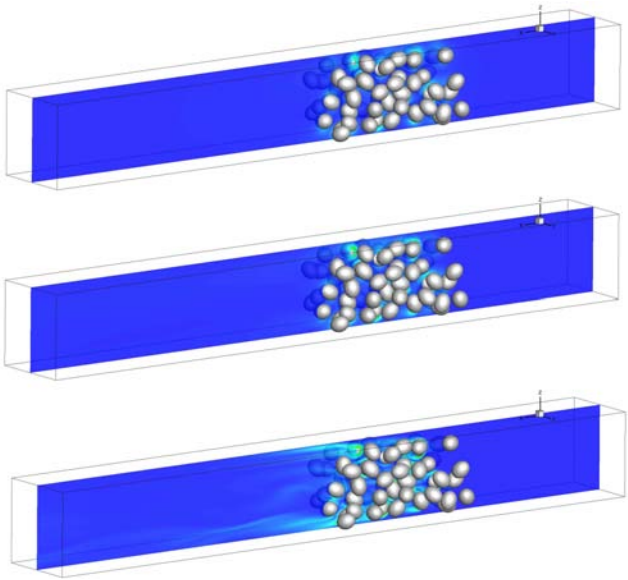

FIGURE 15. EFFECT OF THE PARTICLE REYNOLDS NUMBER ON THE NORMALIZED VORTICITY MAGNITUDE. NON-SPHERICAL PARTICLE FOR $w = 1.25$ AND $\alpha_p = 15\%$. FROM TOP TO BOTTOM: Re_p=1, 10 AND 100.

a new law for the drag coefficient. It has been shown that the present proposal is more accurate than the correlation recently proposed by [7]. The next step of this study would be to confirm the body-fitted results obtained outside the Stokes regime using the fictitious domain approach.

This study has been then extended to the flow through multiple ellipsoidal particles. Direct Numerical Simulations have been carried out for several solid volume fraction, several particle Reynolds number and several aspect ratios. Through these preliminary results, the formation of wakes taking the neighboring particles into account can be showed. Nevertheless, more investigations are necessary to really understand the role of the aspect ratio on the wake production mechanism. The pressure drop has been measured and the results show a decrease when the aspect ratio of the particles is increasing. These preliminary measures of the pressure drop through this lattice of non spherical particles and its connection with the drag coefficient should be more thoroughly analyzed in a further study.

ACKNOWLEDGMENT

This study received funding by ANR-PLAYER; their support is gratefully acknowledged. The work was granted access to the HPC resources of CINES under the allocation x20142b6012 made by GENCI (Grand Equipement National de Calcul Intensif) and of CALMIP under the allocation P0111.

REFERENCES

[1] Jeffery, B., 1922. "The motion of ellipsoidal particles immersed in a viscous fluid". *Proc. R. Soc. London Ser. A,* ***102***, pp. 161–179.

[2] Brenner, H., 1963. "The stokes resistance of an arbitrary particle". *Chem. Eng. Sci.,* ***18***(1), pp. 1–25.

[3] Marchioli, C., Fantoni, M., and Soldati, A., 2010. "Orientation, distribution, and deposition of elongated, inertial fibers in turbulent channel flow". *Physics of fluids,* ***22***, p. 033301.

[4] Chhabra, R., Agarwal, L., and Sinha, N. K., 1999. "Drag on non-spherical particles: an evaluation of availables methods". *Powder Technol,* ***101***, pp. 288–295.

[5] Ouchène, R., Khalij, M., Tanière, A., and Arcen, B., 2013. "Drag, lift and torque coefficients of the ellipsoidal particles". In Euromech Colloquium N505, A. E. nd B. Editor, ed.

[6] Hölzer, A., and Sommerfeld, M., 2008. "New simple correlation formula for the drag coefficient of non-spherical particles". *Powder Technol,* ***184***, pp. 361–365.

[7] Zastawny, M., Mallouppas, G., Zhao, F., and van Wachem, B., 2012. "Derivation of drag and lift force and torque coefficients for non-spherical particles in flows". *Int. Journal of Multiphase flows,* ***101***, pp. 288–295.

[8] Maury, B., 1999. "Direct simulations of 2d fluid-particle flows in biperiodic domains". *Journal of Computational*

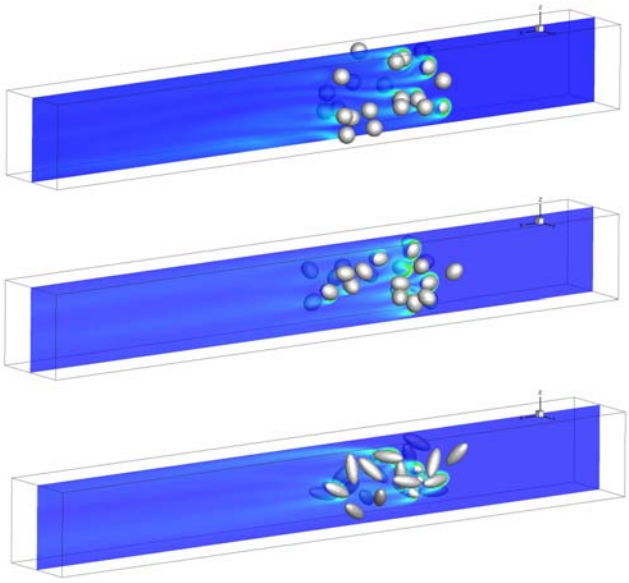

FIGURE 16. EFFECT OF THE ASPECT RATIO ON THE NORMALIZED VORTICITY MAGNITUDE FOR THE NON-SPHERICAL PARTICLE FOR $\alpha_p = 5\%$ AND $Re_p = 100$. FROM TOP TO BOTTOM: w=1.0, 1.25 AND 2.50.

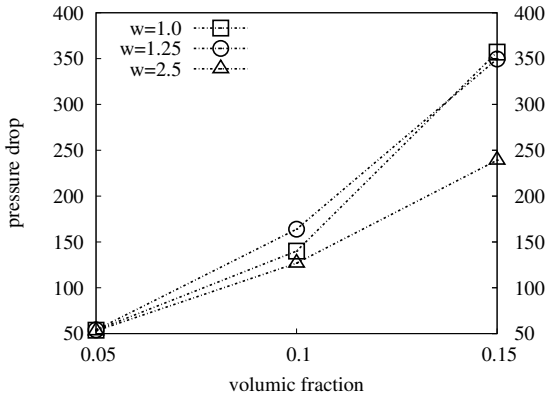

FIGURE 17. PRESSURE DROP THROUGH THE PARTICLES ARRAY FOR $Re_p = 1.0$.

Physics, ***156***(2), pp. 325 – 351.

[9] Khadra, K., Angot, P., Parneix, S., and Caltagirone, J.-P., 2000. "Fictitious domain approach for numerical modelling of navierstokes equations". *International Journal for Numerical Methods in Fluids,* ***34***(8), pp. 651–684.

[10] Mark, A., and van Wachem, B. G., 2008. "Derivation and validation of a novel implicit second-order accurate immersed boundary method". *Journal of Computational Physics,* ***227***(13), pp. 6660 – 6680.

[11] Vincent, S., Sarthou, A., Caltagirone, J.-P., Sonilhac, F., Février, P., Mignot, C., and Pianet, G., 2011. "Augmented lagrangian and penalty methods for the simulation of two-phase flows interacting with moving solids. application to hydroplaning flows interacting with real tire tread patterns". *Journal of Computational Physics,* ***230***(4), pp. 956 – 983.

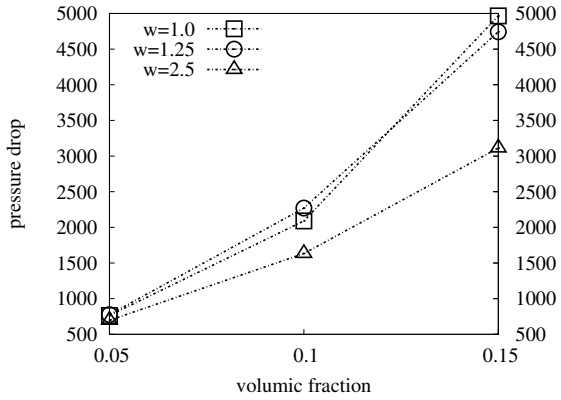

FIGURE 18. PRESSURE DROP THROUGH THE PARTICLES ARRAY FOR $Re_p = 10.0$.

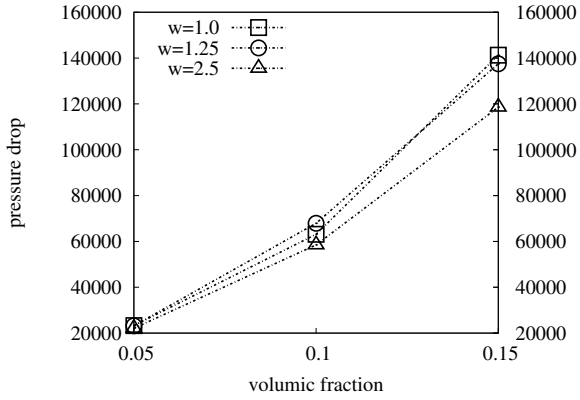

FIGURE 19. PRESSURE DROP THROUGH THE PARTICLES ARRAY FOR $Re_p = 100.0$.

[12] Vincent, S., de Motta, J. C. B., Sarthou, A., Estivalezes, J.-L., Simonin, O., and Climent, E., 2014. "A lagrangian VOF tensorial penalty method for the DNS of resolved particle-laden flows". *Journal of Computational Physics,* ***256***(0), pp. 582 – 614.

[13] Patankar, S., and Spalding, D., 1972. "Mathematical models of fluid flow and heat transfer in furnaces". In A Review, Paper 2, 4th Symposium on Flames and Industry, A. E. nd B. Editor, ed.

[14] Kataoka, I., 1986. "Local instant formulation of two-phase flow". *International Journal of Multiphase Flow,* ***12***(5), pp. 745 – 758.

[15] Johnson, T., and Patel, V., 1999. “Flow past a sphere up to a reynolds number of 300”. *J. Fluid Mech,* ***378***, pp. 19–70.
[16] Loth, E., 2008. “Drag of non-spherical solid particles of regular and irregular shape”. *Powder Technology,* ***182***, pp. 342–353.
[17] Schiller, L., and Naumann, A., 1933. “Fundamental calculations in gravitational processing”. *Zeitschrift Des Vereines Deutscher Ingenieure,* ***77***, pp. 318–320.
[18] Ergun, S., 1952. “Fluid flow through packed columns”. *Chemical Engineering Progress,* ***48***, pp. 89–94.